American Mineralogist, Volume 74, pages 586–592, 1989

Burgers vector determination in clinoamphibole by computer simulation

Randolph J. Cumbest
Department of Geological Sciences, Virginia Polytechnic Institute, Blacksburg, Virginia 24061, U.S.A.
Herman L. M. Van Roermund
Instituut voor Aardwetenschappen, Rijksuniversiteit Utrecht, 3584 CD Utrecht, The Netherlands
Martyn R. Drury
Research School of Earth Sciences, The Australian National University, G.P.O. Box 4, Canberra ACT, Australia
Carol Simpson
Department of Earth and Planetary Sciences, The Johns Hopkins University, Baltimore, Maryland 21218, U.S.A.

Abstract

Diffraction-contrast experiments compared with computer simulation of dislocation images confirm that the primary unit Burgers vector in clinoamphibole is [001]. This information, along with operative glide systems and calculated dislocation energies, is considered in order to propose a possible model for the [001] unit Burgers vector in the clinoamphibole structure.

Introduction

The physical and chemical properties of crystals can often be strongly influenced by their defect content. Potentially, this can result in modification of crystal behavior during geologically important processes such as nucleation (Smith, 1985), chemical reaction (Wintsch and Dunning, 1985), and diffusion (Yund et al., 1983), as well as deformation (White, 1976). The utility of clinoamphibole in both metamorphic and isotopic studies makes important both the characterization of the types of defects it can contain and the influence, if any, of these defects upon its physical and chemical properties.

Experimentally deformed clinoamphibole typically deforms by twinning on $(\bar{1}01)$ in the $C2/m$ setting (Buck, 1970; Rooney et al., 1970, 1975; Morrison-Smith, 1976). Dollinger and Blacic (1975) reported slip on [001](100) based on an analysis of kink bands. From TEM analysis of experimentally deformed clinoamphibole, Morrison-Smith (1976) reported [001](100) as the predominant slip system and suggested that slip on [001](010), [100](010), and [100](001) may also be possible. In contrast, $(\bar{1}01)$ twinning is not reported from naturally deformed specimens except in environments characterized by exceedingly high strain rates (Chao, 1967; Borg, 1972). In their TEM analysis of naturally deformed clinoamphibole, Biermann and Van Roermund (1983) reported [001](100) as the predominant slip system with expanded glide loops consisting mostly of screw segments. Stacking faults on (010) and (100) deformation twins have also been reported (Biermann, 1981; Biermann and Van Roermund, 1983). In naturally deformed samples, subgrain boundaries are typically parallel to $\{hk0\}$ and are reported to consist primarily of screw dislocations parallel to **c** (Biermann and Van Roermund, 1983; Brodie and Rutter, 1985). These previous TEM studies utilized the $\mathbf{g}\cdot\mathbf{b} = 0$ (Hirsch et al., 1965) invisibility criterion for Burgers vector identification, where **g** is the reciprocal lattice vector representing the diffracting planes and **b** is the dislocation Burgers vector. The $\mathbf{g}\cdot\mathbf{b} = 0$ invisibility criterion is strictly true only for pure screw dislocations and for elastically anisotropic crystals (Head et al., 1973). In other situations, it may be necessary to calculate the image by computer-simulation techniques (Head et al., 1973; Gandais et al., 1982) and to compare the computer images with those obtained experimentally. This technique has been applied to olivine (Boland and Buiskoal Toxopeus, 1977), quartz (McCormick, 1976), alkali feldspar (Gandais et al., 1982), and plagioclase (Olsen and Kohlstedt, 1984). In this study we present the results of a TEM study of naturally deformed clinoamphibole that confirms [001] as the primary unit Burgers vector by computer-simulation techniques.

Sample description and experimental techniques

The clinoamphibole in this study is from a mylonitic amphibolite contained within Caledonian successions on the island of Senja, Norway. The rock is compositionally layered, consisting of plagioclase-rich domains interlayered on a millimeter scale with domains enriched in clinoamphibole. The matrix contains a well-developed L-S (linear-planar) fabric defined by preferred alignment of clinoamphibole needles. Within the matrix occur larger clinoamphibole grains with significant amounts of intracrystalline strain and core and mantle structures that are interpreted to be σ_a-type porphyroclasts (Passchier and Simpson, 1986). The clinoamphibole ranges in composition from actinolitic hornblende to tschermakitic hornblende. Based on amphibole compositions, the last stages

0003–004X/89/0506–0586$02.00

of deformation and metamorphism probably occurred at 550 °C and 6.5 kbar. A more detailed account of the sample location and description, in addition to microstructural characteristics, compositional variation, and metamorphic evolution is described in Cumbest et al. (1989).

TEM analysis was carried out at the Institute of Earth Sciences, State University of Utrecht, The Netherlands, using a JEOL 200C fitted with double-tilt stage. Crystallographic orientations of various defects were determined by conventional trace analysis (Hirsch et al., 1965). Burgers vector determination was accomplished by diffraction-contrast experiments using the two-beam technique (Hirsch et al., 1965) in conjunction with computer simulation of defect images using a version of the FORTRAN program TWODIS (Head et al., 1973), modified to accommodate crystal lattices more general than cubic. A description and FORTRAN code for these modifications to TWODIS is available upon request. The intricacies of utilizing this method for crystals with large unit cells are discussed in detail in Montardi and Mainprice (1987) and apply here. It should be noted that the clinoamphibole was found to be extremely stable in the electron beam.

All crystallographic calculations and indexing were done with the lattice parameters and equivalent positions reported for a hornblende by Trojer and Walitzi (1965). The lattice parameters are $a = 0.986$ nm, $b = 1.807$ nm, $c = 0.533$ nm, $\beta = 105.5°$. In calculating the scattering factors for each equivalent position, we used the following composition and site assignments, which are more representative of the clinoamphibole in our study (Cumbest et al., 1989):

$$\underset{(A)}{(K_{0.02}Na_{0.11})}\underset{(M4)}{(Na_{0.03}Ca_{1.86}Mn_{0.03}Fe_{0.08})}-$$

$$\underset{(M1,M2,M3)}{(Fe_{0.86}Mg_{3.75}Ti_{0.02}Al_{0.37})}\underset{(T)}{(Al_{0.53}Si_{7.47})}\underset{(O)}{O_{22}(OH)_2}.$$

Using these data, calculated extinction distances for some reflections commonly used in this study are reported in Table 1. Elastic constants used for calculating defect images are those for hornblende II (Alexandrov and Ryzhova, 1961), as reported in Birch (1966). However, Alexandrov and Ryzhova (1961) reported no composition for either hornblende I or hornblende II. It was found during the course of the study that hornblende II gave the best match to observed images.

The input parameters to TWODIS are described in detail in Head et al. (1973). However, a brief description will be given below so that the images can be compared with a minimal amount of effort. The input parameters that characterize the dislocation are the Burgers vector (**b**) and dislocation line direction (**u**); **b** and **u** are specified in terms of direct lattice vectors [*uvw*]. The TEM sample is a very thin foil that can be geometrically approximated by a thin slab. The orientation of this slab with respect to the crystal lattice is characterized by the foil normal (FN), a vector normal to the surface of the slab that makes an obtuse angle with the electron flux. Since the specimen can be tilted in the microscope, the FN and electron flux are not generally parallel. FN is specified in terms of a reciprocal lattice vector *hkl*. The thickness of the slab (THICK) is specified in terms of extinction distance. Since the extinction distance is a function of, among other things, the operating two-beam diffraction condition, THICK changes with the diffraction vector, although the true thickness of the slab remains constant. The anomalous absorption coefficient (ANO) determines how the electron beam is attenuated within the foil and has the practical effect on the image of causing the defect contrast to be attenuated in the center of the foil (i.e., the center of the image) as the value of ANO is increased. ANO is determined by trial and error by comparing computed images with electron micrographs. The orientation of the specimen with respect to the electron microscope is given by the electron-beam orientation (BM) and is expressed in terms of the direct lattice vector [*uvw*] that is, by convention, opposite in direction to the electron flux. The diffraction condition is specified in terms of the reciprocal lattice vector $\mathbf{g} = hkl$, representing the diffracting planes and the dimensionless deviation parameter (w) that describes the distance from the exact Bragg condition for these planes. The parameters START and FINISH control the framing and magnification of the computed image.

TABLE 1. Calculated extinction distances for selected diffraction conditions

Diffraction vector **g**	Calculated extinction distance ϵ_g (nm)
002	38.4
$\bar{2}02$	38.4
$\bar{4}04$	82.4
020	20.3
200	25.2
110	20.9

TEM ANALYSIS

TEM analysis of clinoamphibole porphyroclasts revealed relatively high defect densities (5×10^8 cm^{-2}), including high densities of free dislocations, dislocation arrays, subgrain boundaries, and planar defects. Most of the free dislocations consist of long straight segments. However, dark-field, weak-beam images (Fig. 1, arrowed a) show that even where curved segments are present, the line directions show strong crystallographic control. Trace analysis of line directions (Fig. 2) for free dislocations show strong point maxima that indicate that most of these are subparallel to **c** or lie on planes between (110) and ($1\bar{1}0$).

Dislocations showed the most well-defined contrast when imaged with $\mathbf{g} = \bar{2}02$. Figure 3 shows free dislocations imaged with $\mathbf{g} = \bar{2}02$ along with computer-simulated images for all possible unit dislocations in the cli-

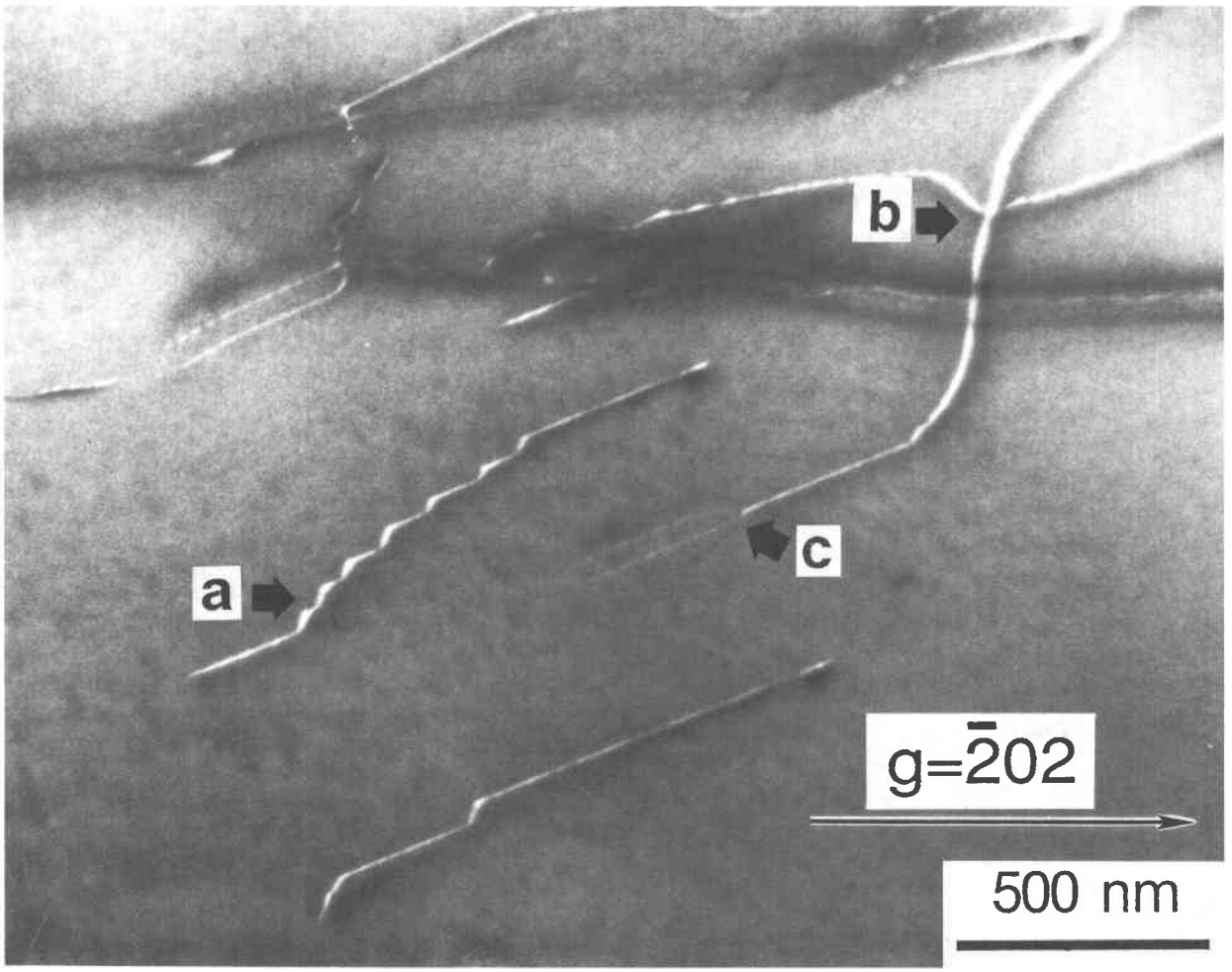

Fig. 1. Dark-field, weak-beam electron micrograph ($s_g = 1.3 \times 10^{-1}$ nm, $w = 4.85$) of free dislocations showing strong crystallographic control on dislocation line directions (arrowed a), interaction of dislocations on different glide planes (arrowed b), and dissociation of unit dislocations (arrowed c). BM = [010].

noamphibole structure. Since the left ends of the dislocations showed the most detailed contrast effects, the computer-simulated images were calculated with this part of the dislocation enlarged to provide maximum detail for comparison. The [010] Burgers vector can be immediately excluded because the detailed character of its computed image is significantly different from the contrast in the TEM micrograph (Fig. 3). The qualitative difference between the remaining possible Burgers vectors is not as great, and exclusion of any of the others based on this diffraction condition alone would be disputed.

Two-beam analysis of these dislocations for three different diffraction conditions are shown in Figure 4, along with associated computer-simulated images for all possible unit dislocations in the clinoamphibole structure. It should be kept in mind that, in matching computed images to the electron micrographs, it is consistent to rotate the computed image 180° about a vertical axis if necessary since this only results in changing the sign of the diffraction vector (Head et al., 1973). Also, the image width of a dislocation is approximately one third the extinction distance effective for the image-diffraction conditions (Hirsch et al., 1965, p. 253). For the diffraction conditions $\mathbf{g} = 0\bar{2}0$ and $\mathbf{g} = \bar{1}\bar{1}0$, the dislocation images appear narrower since the extinction distances for these diffraction conditions are shorter than for $\mathbf{g} = \bar{2}02$.

For $\mathbf{g} = \bar{2}02$, all experimental images show significant contrast. However, for $\mathbf{g} = 0\bar{2}0$ and $\mathbf{g} = \bar{1}\bar{1}0$, dislocations show extremely weak contrast in the TEM micrographs. The computer-simulated images for $\mathbf{g} = 0\bar{2}0$ and $\mathbf{g} = \bar{1}\bar{1}0$ show significant amounts of contrast for all Burgers vectors other than $\mathbf{b} = [001]$. For $\mathbf{g} = 0\bar{2}0$ and $\mathbf{g} = \bar{1}\bar{1}0$ with $\mathbf{b} = [001]$, the computer-simulated images show very weak contrast at the tips of the dislocations only. Therefore, matching the computed images with these diffraction conditions reveals that the [001] Burgers vector is the best match between computed images and electron micrographs. The facts that most dislocation line directions are

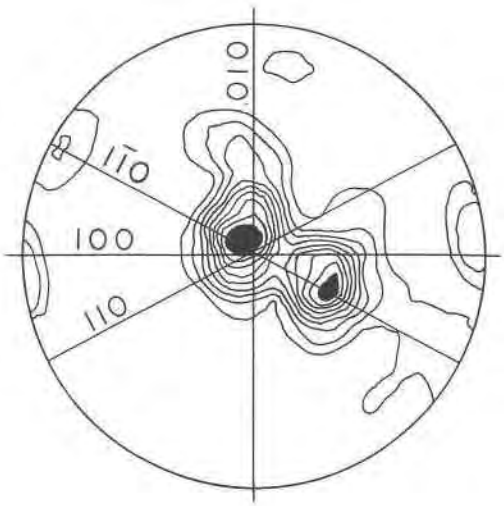

Fig. 2. Contoured, upper-hemisphere, equal-area stereographic projection of dislocation line directions. **c** is vertical. Contoured at 1, 2, 3, 4, 5, 6, 7, 8, and 9 points per 2.3% area; 43 data points.

subparallel to **c** (Fig. 2) and [001] is the Burgers vector indicate that most dislocations have predominantly screw character.

Discussion

The predominance of the [001] Burgers vector in the clinoamphibole structure is consistent with **c** being the shortest unit translation (i.e., 0.533 nm for **c** compared with 0.986 nm for **a** and 1.807 nm for **b**). Because the energy of a dislocation is proportional to the square of the length of its Burgers vector (Hull and Bacon, 1984), [001] will be by far the most energetically favored unit Burgers vector. It is also the one most commonly reported (Morrison-Smith, 1976; Biermann and Van Roermund, 1983). However, Morrison-Smith (1976) also reported the possible existence of [100] as a Burgers vector for hornblende crystals that were experimentally deformed at a strain rate of 10^{-5} s^{-1} and temperatures up to 600 °C.

The structure and crystal chemistry of clinoamphiboles are reviewed in detail by Hawthorne (1985). Figure 5a

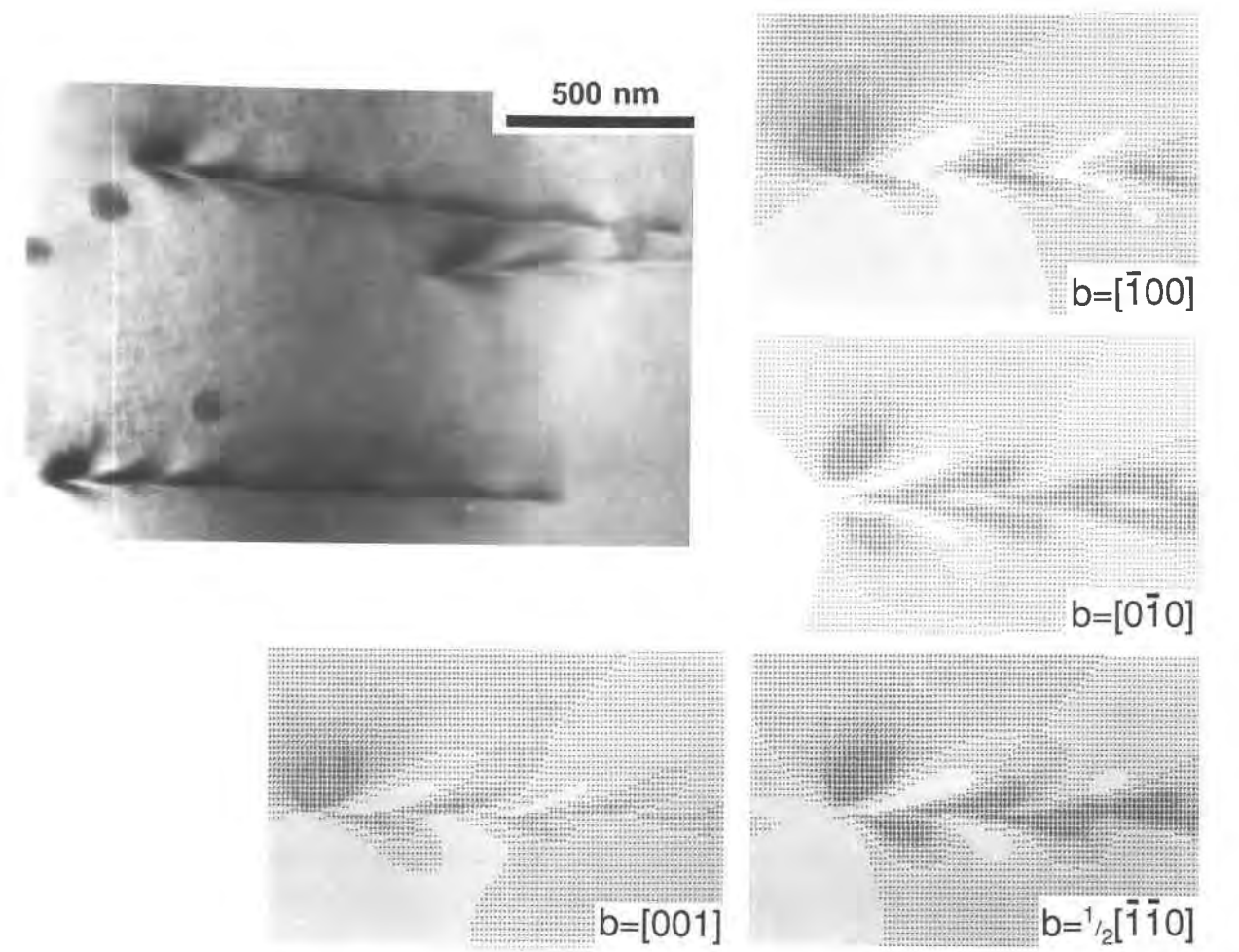

Fig. 3. Bright-field electron micrograph of free dislocations with accompanying computer-simulated images for **g** = $\bar{2}$02 and indicated Burgers vectors. Parameters used for computer-simulated images are **u** = [$\bar{1}\bar{1}$5]; FN = ($\bar{2}$2$\bar{1}$); ANO = 0.07; START = 3.25; FINISH = 6.75; THICK = 6.25; BM = [$\bar{1}$01]; w = 0.05.

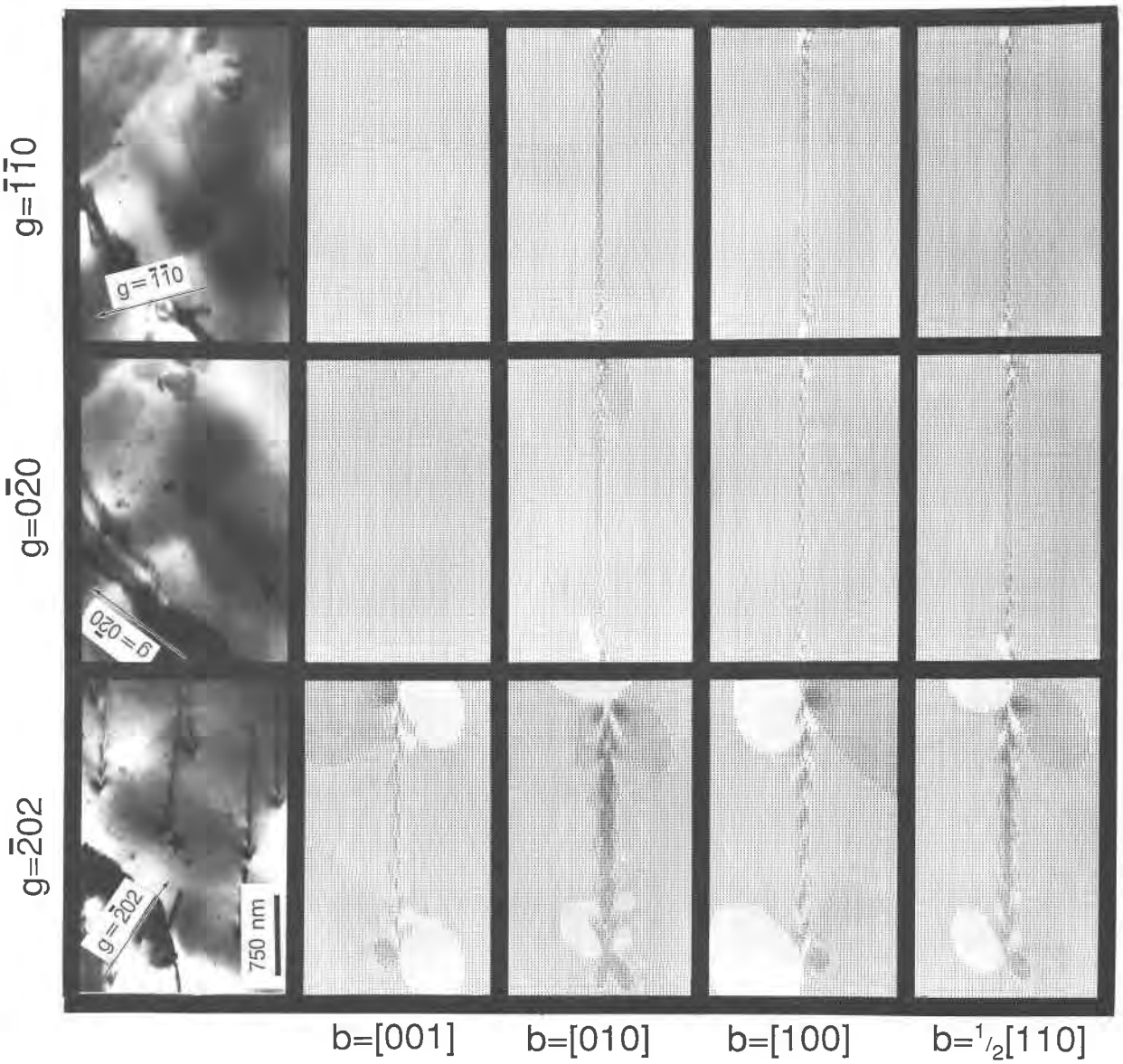

Fig. 4. Bright-field electron micrographs of free dislocations with accompanying computer-simulated images for indicated diffraction conditions and Burgers vectors. Parameters used for computing simulated images are $\mathbf{u} = [\bar{1}\bar{1}\bar{5}]$; FN = $(\bar{2}2\bar{1})$; ANO = 0.07. For $\mathbf{g} = \bar{2}02$, START = −1.00; FINISH = 7.25; THICK = 6.25; BM = $[\bar{1}0\bar{1}]$; $w = 0.05$. For $\mathbf{g} = 0\bar{2}0$, START = −1.00; FINISH = 12.82; THICK = 11.82; BM = $[\bar{1}0\bar{1}]$; $w = 0.03$. For $\mathbf{g} = \bar{1}\bar{1}0$, START = −1.00; FINISH = 12.54; THICK = 11.54; BM = $[\bar{1}\bar{1}\bar{2}]$; $w = 0.03$. Stars mark the same reference point in each photograph.

shows the undeformed clinoamphibole structure projected onto (100). If the M2–O4 and M4–O4 bonds were broken and the T2 tetrahedron translated along the [001] direction (Fig. 5b) to the equivalent lattice position, this would leave the T2 tetrahedron that was originally bonded to M2B now unbonded, creating an extra half plane in the clinoamphibole structure and a dislocation defined by $\mathbf{b} = [001]$. The illustration in Figure 5b is meant to be schematic and intended only to illustrate the relative movements of the structural units. The strain associated with the [001] translation will be distributed more uniformly in the crystal lattice proximal to the dislocation core than is shown in Figure 5b, as indicated by the occurrence of significant contrast in the electron micrographs.

Figure 6 illustrates the "I-beam" representation of the clinoamphibole structure projected onto (001). Possible configurations for the slip plane in the (110) and (100) planes are also shown. The configurations result from jogs in the dislocation line around the "I-beams" so that only

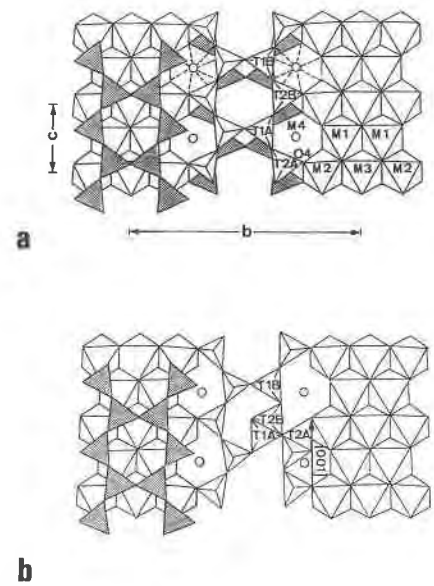

Fig. 5. Schematic illustration for possible configuration of [001] Burgers vector in the clinoamphibole structure viewed down (100) (adapted from Hawthorne, 1985). (**a**) Undeformed lattice. (**b**) Lattice with [001] Burgers vector. Downward-pointing tetrahedra stippled; displaced upward-pointing tetrahedra black.

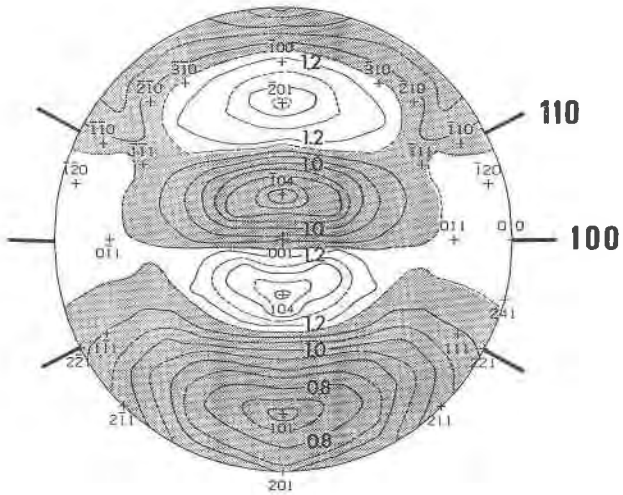

Fig. 7. Contoured, upper-hemisphere projection of calculated dislocation energies for **b** = [001]. Contour intervals are in terms of $\ln(r/r_0) \times 10^{-9}$ N where r and r_0 are the inner- and outer-cutoff radii, respectively (see Hirth and Lothe, 1969, p. 62–63). Shaded areas denote levels below 1.15. Traces of selected lattice planes indicated.

the 6-coordinated (M2) and 8-coordinated (M4) bonds are disrupted, and possibly also the 12-coordinated "A" site. For a unit dislocation, this configuration seems energetically more favorable than a dislocation line passing through the layer of 6-coordinated (M1,M2,M3) cations that bond the double chains. It is also apparent from Figure 6 that with the dislocation line configuration illustrated, no tetrahedral bonds will be broken by movement of the dislocations. Similar arguments would apply to any glide plane between (110) and (1$\bar{1}$0). However, the {110} glide planes should have slightly lower dislocation energies per unit length since the repeat in the [110] direction is slightly longer than the repeat in the [100] direction. Therefore, for dislocations with the same amount of edge or screw character, a dislocation on a {110} plane should disrupt fewer bonds per unit length than a dislocation lying on a plane closer to (100). Figure 7 illustrates calculated dislocation energies using the program of Head et al. (1973, p. 329) for the [001] Burgers vector versus the dislocation line direction. As this diagram shows, dislocation energies become progressively less as the plane containing the dislocation goes from {110} to (100). The pattern is not simple, however, as dislocation energies in the (010) plane show several minima and maxima. The minimum in the [$\bar{1}$04] orientation corresponds approximately to the maximum in the number of dislocations subparallel to **c** observed in the natural sample (Fig. 2).

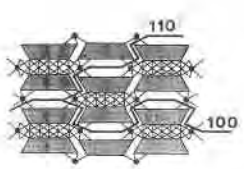

Fig. 6. Schematic illustration of possible location of slip planes in clinoamphibole structure projected onto (001) (adapted from Hawthorne, 1985). Black dots indicate locations of M4 sites.

Acknowledgments

This study was supported by National Science Foundation grant EAR 8606120 to Carol Simpson. Brad K. Smith provided a version of the program TWODIS. The final manuscript benefited from reviews by K. H. Brodie and Paul H. Ribbe. Llyn Sharp provided technial assistance with photography.

References cited

Alexandrov, K.S., and Ryzhova, T.V. (1961) The elastic properties of rock-forming minerals: Pyroxenes and amphiboles. Izvestya Geophysics, Ser. 9, 1339–1344.

Biermann, C. (1981) (100) Deformation twins in naturally deformed amphiboles. Nature, 292, 621–633.

Biermann, C., and Van Roermund, H.L.M. (1983) Defect structures in naturally deformed clinoamphibole—A TEM study. Tectonophysics, 95, 267–278.

Birch, F. (1966) Compressibility; elastic constants. Geological Society of America Memior 97, 97–173.

Boland, J.N., and Buiskoal Toxopeus, J.M.A. (1977) Dislocation deformation mechanisms in peridotite xenoliths in kimberlites. Contributions to Mineralogy and Petrology, 60, 17–30.

Borg, I.Y. (1972) Some shock effects in granodiorite to 270 Kb. at the Piledriver site. Geophysical Monographs of the American Geophysical Union, 16, 293–311.

Brodie, K.H., and Rutter, K.H. (1985) On the relationship between deformation and metamorphism, with special reference to the behavior of basic rocks In A.B. Thompson and D.C. Rubie, Eds., Metamorphic reactions: Kinetics, textures, and deformation, p. 139–179. Springer-Verlag, New York.

Buck, P. (1970) Verformung von Hornblende-Einkristallen bei Drucken bis 21 kb. Contributions to Mineralogy and Petrology, 28, 62–71.

Chao, E.C.T. (1967) Shock effects in certain rock-forming minerals. Science, 156, 192–202.

Cumbest, R.J., Drury, M.R., Van Roermund, H.L.M., and Simpson, C. (1989) Dynamic recrystallization and chemical evolution of clinoamphibole from Senja, Norway. Contributions to Mineralogy and Petrology, in press.

Dollinger, G., and Blacic, J.D. (1975) Deformation mechanisms in experimentally and naturally deformed amphiboles. Earth and Planetary Science Letters, 26, 409–416.

Gandais, M., Hiki, A., Willaime, C., and Epelboin, Y. (1982) Dislocation contrast by transmission electron microscopy. A method for Burgers vector determination if the invisibility criterion is not valid. Philosophical Magazine, A45, 387–400.

Hawthorne, F.C. (1985) Crystal chemistry of the amphiboles. Mineralogical Society of America Reviews in Mineralogy, 9A, 1–102.

Head, A.K., Humble, P., Clarebrough, L.M., Morton, A.J., and Forwood, C.T., Eds. (1973) Computed electron micrographs and defect identification. Defects in crystalline solids, 7, 400 p. North Holland, Amsterdam.

Hirsch, P.B., Howie, A., Nicholson, R.B., Pashley, P.W., and Whelan, M.J. (1965) Electron microscopy of thin crystals, 549 p. Butterworths, Washington.

Hirth, J.P., and Lothe, J. (1969) Theory of dislocations, 780 p. McGraw-Hill, New York.

Hull, D., and Bacon, D.J. (1984) Introduction to dislocations (3rd edition), 257 p. Pergamon Press, Oxford.

McCormick, J.W. (1976) Computer simulation of dislocation images in quartz. In H.R. Wenk, Ed., Electron microscopy in mineralogy, p. 113–122. Springer-Verlag, Berlin.

Montardi, Y., and Mainprice, D. (1987) A transmission electron microscope study of the natural plastic deformation of calcic plagioclases. Bulletin de Minéralogie, 110, 1–14.

Morrison-Smith, D.J. (1976) Transmission electron microscopy of experimentally deformed hornblende. American Mineralogist, 61, 272–280.

Olsen, T.S., and Kohlstedt, D.L. (1984) Analysis of dislocations in some naturally deformed plagioclase feldspars. Physics and Chemistry of Minerals, 11, 153–160.

Passchier, C.W., and Simpson, C. (1986) Porphyroclast systems as kinematic indicators. Journal of Structural Geology, 8, 831–843.

Rooney, T.P., Rieker, R.E., and Ross, M. (1970) Deformation twins in hornblende. Science, 169, 173–175.

Rooney, T.P., Riecker, R.E., and Gavasci, A.T. (1975) Hornblende deformation features. Geology, 3, 364–366.

Smith, B.K. (1985) The influence of defect crystallography on some properties of orthosilicates. In A.B. Thompson and D.C. Rubie, Eds., Metamorphic reactions: Kinetics, textures, and deformation, p. 98–117. Springer-Verlag, New York.

Trojer, F., and Walitzi, E.M. (1965) Strukturuntersuchung an einer Hornblende aus dem eklogitischen Gestein von Stramez, südliche Koralpe. Tschermaks Mineralogische und Petrographische Mitteilungen, 10, 233–240.

White, S.H. (1976) The effects of strain on the microstructure, fabrics, and deformation mechanisms in quartz. Philosophical Transactions of the Royal Society of London, A282, 69–86.

Wintsch, R.P., and Dunning, J. (1985) The effect of dislocation density on the aqueous solubility of quartz and some geologic implications: A theoretical approach. Journal of Geophysical Research, 90, 3649–3657.

Yund, R.A., Smith, B.M., and Tullis, J. (1983) Dislocation—Assisted diffusion of oxygen in albite. Physics and Chemistry of Minerals, 7, 185–189.

Manuscript received July 7, 1988
Manuscript accepted January 20, 1989